1 **TITLE:**

2 Transmembrane polar relay drives the allosteric regulation for ABCG5/G8 sterol transporter.

3 **AUTHOR NAMES:**

4 *Bala M. Xavier[1,‡,#], Aiman A. Zein[1,‡,#], Angelica Venes[1,2], Junmei Wang[3,*] and Jyh-Yeuan Lee[1,*]*

5 **AUTHOR ADDRESS:**

6 [1] Department of Biochemistry, Microbiology and Immunology, Faculty of Medicine & [2]
7 Biomedical Sciences Program, Department of Biology, Faculty of Science, University of Ottawa,
8 Ontario, Canada, K1H 8M5. [3] Department of Pharmaceutical Sciences, School of Pharmacy,
9 University of Pittsburgh, Pittsburgh, PA 15261, USA.

10 **KEYWORDS:**

11 ABCG5, ABCG8, ATP-binding cassette transporter, cholesterol, polar relay, sitosterolemia

12 **AUTHOR INFORMATION**

13 * Correspondence should be addressed to Junmei Wang (junmei.wang@pitt.edu) and Jyh-Yeuan
14 (Eric) Lee (Jyh-Yeuan.Lee@uOttawa.ca).

15 ‡ Contributed equally.

16 # Current address: Department of Cellular and Molecular Medicine, Faculty of Medicine,
17 University of Ottawa

18

ABSTRACT:

The heterodimeric ATP-binding cassette (ABC) sterol transporter, ABCG5/G8, is responsible for the biliary and transintestinal secretion of cholesterol and dietary plant sterols. Missense mutations of ABCG5/G8 can cause sitosterolemia, a loss-of-function disorder characterized by plant sterol accumulation and premature atherosclerosis. A new molecular framework was recently established by a crystal structure of human ABCG5/G8 and reveals a network of polar and charged amino acids in the core of the transmembrane domains, namely polar relay. In this study, we utilize genetic variants to dissect the mechanistic role of this transmembrane polar relay in controlling ABCG5/G8 function. We demonstrated a sterol-coupled ATPase activity of ABCG5/G8 by cholesteryl hemisuccinate (CHS), a relatively water-soluble cholesterol memetic, and characterized CHS-coupled ATP catalysis by using three loss-of-function missense variants, two sitosterolemia mutations (E146Q and R543S; within polar relay) and one sterol-binding mutation (A540F; distant from the polar relay). The results established an *in vitro* phenotype of the loss-of-function and missense mutations of ABCG5/G8, showing significantly impaired ATPase activity and loss of energy sufficient to weaken the polar relay network by all three mutants. Our data herein provide a biochemical evidence underlying the importance of the polar relay in regulating the catalytic activity of ABCG5/G8 sterol transporter.

37 **INTRODUCTION**

38 All living cells depend on the ability to translocate nutrients, metabolites, and other
39 molecules across their membranes. One major way to achieve this is through membrane-
40 anchored transporter proteins. The evolutionarily conserved ATP-binding cassette (ABC)
41 transporter superfamily, for example, carry out ATP-dependent and active transport of a wide
42 range of substances across cellular membranes, including both hydrophilic and hydrophobic
43 molecules such as sugars, peptides, antibiotics, or cholesterol (Dean et al., 2001; Dean and
44 Allikmets, 1995; Hwang et al., 2016; Linton and Higgins, 1998). As a key component of cellular
45 membranes, cholesterol constitutes ~50% of cellular lipid content; it is also the precursor of
46 steroid hormones that modulate gene regulation and bile acids that enable nutrient absorption.
47 Translocation of cholesterol molecules on biological membranes plays an essential role in
48 maintaining cellular and whole-body cholesterol homeostasis. Thus, excess cholesterol needs to
49 be eliminated from cells and tissues through either sterol acceptors in the circulation or direct
50 excretion into the bile or the gut (Li et al., 2013; Patel et al., 2018). A large body of evidence
51 indicates that ABC sterol transporters regulate cholesterol metabolism, and their defects are
52 associated with dysregulation of whole-body cholesterol homeostasis, a major risk factor for
53 cardiovascular diseases (Borst et al., 2000; Xavier et al., 2019). Yet we have almost no
54 understanding of how these transporters actually translocate cholesterol molecules and how the
55 sterol-transport process is controlled by ATP catalysis. Given the dysregulation of cholesterol
56 metabolism as a major risk factor for cardiovascular disease, there is a pressing need to elucidate
57 of mechanism of these transporters in moving molecules across the cell membranes.

58 Recent progress in solving a heterodimeric crystal structure of human ABCG5 and
59 ABCG8 establishes a new molecular framework towards such a mechanistic understanding of

60 ABC sterol transporters. ABCG5 and ABCG8 are half-sized ABC sterol transporters and co-
61 expressed on the apical surface of the hepatocytes along the bile ducts and the enterocytes from
62 the intestinal brush-boarder membranes (Graf et al., 2003, 2002). ABCG5 and ABCG8 function
63 as obligate heterodimers (ABCG5/G8) and serve as the primary and indispensable sterol-efflux
64 pump that effectively exports excess cholesterol, non-cholesterol sterols, and dietary plant sterols
65 into the bile and the intestinal lumen. In mammals, most cholesterol is eliminated by its
66 metabolism into bile acids or via biliary secretion as free cholesterol. The latter is considered as
67 the last step of reverse cholesterol transport (RCT), where ABCG5/G8 accounts for more than
68 75% biliary cholesterol secretion (Bhattacharyya et al., 1991; Klett et al., 2004; Plösch et al.,
69 2004; Yu et al., 2002). Recent studies have shown that in human subjects and animal models,
70 ABCG5/G8 is also responsible for eliminating neutral sterols by the transintestinal cholesterol
71 efflux (TICE), a cholesterol-lowering process independent of RCT (Jakulj et al., 2016).
72 Physiologically, ABCG5/G8 thus plays an essential role in controlling cholesterol homeostasis in
73 our bodies.

74 In general, the smallest functional unit of an ABC transporter consists of two
75 transmembrane domains (TMD1 and TMD2) and two nucleotide-binding domains (NBD1 and
76 NBD2), and both NBDs concertedly bind and hydrolyze ATP to provide the energy and drive
77 substrate transport. The TMDs, on the other hand, have shown to share low sequence similarity
78 in the amino acid sequences and three-dimensional structural folds, suggesting substrate-specific
79 mechanisms for individual transporters (Ford and Beis, 2019). Mechanistic analyses of ABC
80 cholesterol transporters have largely centered on sequence requirement at the canonical ATP-
81 binding sites (Hirayama et al., 2013; Takahashi et al., 2006; Wang et al., 2011; Zhang et al.,
82 2006), whereas limited is known about sterol-protein interaction and its relationship with the

83 ATP catalysis. Recent progress solving a crystal structure of human ABCG5/G8 revealed a
84 unique TMD fold and several structural motifs (Lee et al., 2016). Of particular, for each subunit,
85 a network of polar and charged amino acids is present in the core of the TMD, namely polar
86 relay, whose role remains to be characterized. A triple-helical bundle is located at the
87 transmission interface between the NBD and the TMD and consists of an elbow connecting
88 helix, a hot-spot helix (also known as E-helix), and an intracellular loop-1 (ICL1) coupling helix.
89 However, on the triple-helical bundle or the transmembrane polar relay, several residues have
90 been shown to bear disease-causing missense mutations from sitosterolemia or other metabolic
91 disorders with lipid phenotypes (**Figure 1A**). Notably, several disease-causing mutations are
92 clustered in the membrane-spanning region or at the NBD-TMD interface (Xavier et al., 2019;
93 Zein et al., 2019). This suggests the unique roles of these structural motifs in regulating the
94 ABCG5/G8 function; yet, no prior knowledge was available to explain the role of these
95 structural motifs in the sterol-transport function.

96 Loss-of-function (LOF) mutations in ABCG5 or ABCG8 are linked to sitosterolemia, a
97 rare autosomal recessive disease, while several other missense mutations are also associated with
98 other lipid disorders, such as gallstone formation or elevated LDL cholesterol (Berge et al., 2000;
99 Buch et al., 2007; Chen et al., 2008; Kajinami et al., 2004; Kuo et al., 2008; Lu et al., 2001). At
100 the cellular level, many of the missense mutations lead to defects in post-translational trafficking
101 of ABCG5/G8 from the endoplasmic reticulum (ER), an abnormality commonly observed in
102 other ABC transporters with missense mutations, *e.g.*, DF508 mutation in the cystic fibrosis
103 transmembrane conductance regulator (CFTR or ABCC7) (Graf et al., 2004; Lukacs et al.,
104 1994). However, specific missense mutants of ABCG5/G8 heterodimers have shown no defect in
105 protein maturation (Graf et al., 2004), suggesting alternative disease-causing mechanisms.

106 Therefore, studies of these mutants will not only show how they alter the transporter activity, but
107 will also provide mechanistic insights into the function of wild-type (WT) ABCG5/G8 sterol
108 transporter.

109 Disease mutations are instrumental in studying the mechanisms of affected proteins *in*
110 *vitro*, *e.g.*, familial hypercholesterolemia mutations for proteins involved in low-density
111 lipoprotein metabolism (Kizhakkedath et al., 2019). Guided by the structural framework of
112 ABCG5/G8, we can now investigate its mechanisms using enzymological approaches with
113 purified proteins. For this, we first need to establish at least one robust and consistent *in vitro*
114 functional assay. Using ATPase activity as the functional benchmark in this study, we have
115 optimized an *in vitro* colorimetric ATPase assay that allows high-throughput activity assessment
116 of detergent-purified ABCG5/G8. Using a soluble cholesterol memetic, cholesteryl
117 hemisuccinate (CHS), we report here the CHS-stimulated ATP hydrolysis by ABCG5/G8 proteo-
118 micelles, consisting of phospholipids, cholate, and dodecyl-maltoside (DDM), and present an
119 enzymatic analysis for the sterol-coupled ATPase activity on ABCG5/G8 sterol transporter.
120 Using ATPase activity as functional readout of ABCG5/G8, we show differentially inhibition of
121 the CHS-stimulated ATPase activity by three LOF missense mutants, two sitosterolemia
122 mutations and one sterol-binding mutation, where residues bearing the two disease mutations are
123 located along the polar relay. Our data hereby demonstrate the mechanistic basis on regulating
124 ABCG5/G8 function by the transmembrane polar relay (**Figure 1B**).

125

126 **RESULTS**

127 ***CHS stimulates ATP hydrolysis by wild-type (WT) ABCG5/G8.*** Despite the known
128 physiological role of ABCG5/G8 in biliary and intestinal cholesterol secretion, the direct
129 evidence of sterol-coupled transporter activity was not available. In this study, we investigated
130 sterol-coupled ATPase activity by using CHS, a cholesterol mimetic that is more soluble in
131 aqueous solution. First, to overcome low sensitivity of detecting the ABCG5/G8 ATPase activity
132 by previous protocols, we have optimized the ATPase assay for ABCG5/G8 by adopting a
133 colorimetric bismuth citrate-based detection approach (Cariani et al., 2004), as described in
134 Materials and Methods. This assay significantly reduces the background noise due to cloudiness
135 by phospholipid/cholate/DDM mixtures, which improves the detecting sensitivity of liberated
136 inorganic phosphate within the first few minutes and allows us to calculate more accurate rates
137 of ATP hydrolysis. We show here that CHS can significantly stimulate ABCG5/G8-mediated
138 ATP hydrolysis when co-incubated with sodium cholate (a bile acid) and *E. coli* polar lipids
139 (**Figure 2**). Using 5 mM of ATP, the basal activity of ABCG5/G8 was calculated as 160 ± 15
140 nmol/min/mg (n = 4), similar to reported values, whereas in the presence of CHS, the specific
141 ATPase activity of ABCG5/G8 reached 565 ± 30 nmol/min/mg (n = 8), three-four times higher
142 than that in the absence of CHS (**Figures 3A & 3B**). The activity was inhibited either by
143 orthovanadate, an ATPase inhibitor (Davies and Hol, 2004) (**Figure 3C**), or by a catalytically-
144 deficient mutant $ABCG5_{WT}/G8_{G216D}$ (G8-G216D) (Zhang et al., 2006), which displayed no ATP
145 hydrolysis (**Figures 3A & 3B**).

146 ***The lipid environments fine-tune ABCG5/G8 ATPase activity.*** ABC transporters need to
147 function in phospholipid-embedded environment. However, it is unknown whether the

148 ABCG5/G8 function is controlled by phospholipids of specific headgroups or in specific lipid
149 compositions. Because a high concentration of bile acids is required to activate ABCG5/G8
150 ATPase activity, attempts to use reconstituted proteoliposomes failed due to the immediate
151 solubilization of the reconstituted proteins. To facilitate the assessment of mutant functions, we
152 evaluated the lipid environments to obtain the most optimal assay conditions. To study the effect
153 of lipid conditions and phospholipid species on the ABCG5/G8 function, we analyzed the CHS-
154 coupled ATPase activity in the presence of two polar lipid extracts under a condition of fixed
155 concentrations of sodium cholate and CHS (Materials and Methods). Using *E. coli* polar lipids,
156 we carried out ATP concentration-dependent ATPase assay to determine the Michaelis-Menten
157 kinetic parameters of CHS-stimulated ATP hydrolysis. We have observed the maximal ATP
158 hydrolysis by ABCG5/G8 at concentrations slightly over 2.5 mM of ATP with a V_{max} of 677.1 ±
159 25.6 nmol/min/mg, a K_M(ATP) of 0.60 mM, and a k_{cat} of 1.69 s^{-1}. When using bovine liver polar
160 lipids, we observed ~3.5-fold lower catalytic rate of ATP hydrolysis and ~50% higher K_M(ATP)
161 (**Figure 4A & Table 1**). To determine the dependence of phospholipid headgroups, we tested
162 three most abundant phospholipids in either lipid extract on the ATP hydrolysis by ABCG5/G8,
163 *i.e.,* phosphatidylethanolamine (PE), phosphatidylcholine (PC), and phosphatidylglycerol (PG)
164 (see Materials and Methods). Preincubation with egg PE resulted in the highest specific activity,
165 while the use of soy PC or egg PG only led to slightly higher ATP hydrolysis than the basal
166 activity (**Figure 4B**). Interestingly, PE alone was sufficient to enhance ATP hydrolysis to almost
167 the same level as *E. coli* polar lipids, which was higher than that of liver polar lipid mixture.

168 ***Missense mutants impair CHS-coupled ATPase Activity of ABCG5/G8.*** Using the CHS-
169 coupled ATPase activity as the functional readout, we initiated studies in the catalytic
170 mechanism of ABCG5/G8 by exploiting the transporter's missense mutations that undergo

171 proper trafficking to post-ER cell membranes (ER-escaped mutants). In this study, we have used
172 *Pichia pastoris* yeast and expressed recombinant proteins of G8-G216D, a catalytically deficient
173 mutant, $ABCG5_{E146Q}/G8_{WT}$ (G5-E146Q) and $ABCG5_{WT}/G8_{R543S}$ (G8-R543S), two loss-of-
174 function/sitosterolemia missense mutants, and $ABCG5_{A540F}/G8_{WT}$ (G5-A540F), a loss-of-function
175 mutant with putative sterol-binding defect (**Figure 1B & Supplementary Figure 1**).The purified
176 mutants were preincubated with *E. coli* polar lipids and sodium cholate as described above. The
177 sitosterolemia missense mutants, G5-E146Q and G8-R543S, show a ~80% reduction of the
178 specific activity in CHS-coupled ATP hydrolysis when compared to WT, 160±15 nmol/min/mg
179 and 150 ± 5 nmol/min/mg respectively. The sterol-binding mutant G5-A540F shows a ~90%
180 reduction of ATP hydrolysis, 90 ± 10 nmol/min/mg (**Figure 5**). We then performed ATP
181 concentration-dependent experiments and analyzed the Michaelis-Menten kinetics for these three
182 mutants. For all mutants, K_M(ATP) remained nearly the same as compared to WT, but the
183 mutants displayed a 40-60% reduction in the catalytic rate (**Table 1**). This result suggests that
184 other molecular events, *e.g.*, sterol-transporter interaction, may have a more profound impact on
185 ATPase activity than the nucleotide association.

186 The effects of CHS on ABCG5/G8 WT and mutants were further investigated by measuring the
187 ATP hydrolysis in the CHS concentration-dependent manner at a saturated ATP concentration
188 (5mM here). Purified proteins were preincubated with *E. coli* polar lipids, sodium cholate and a
189 wide range of CHS concentrations (0.064mM - 4.1mM). For WT, we obtained a V_{max} of 702.9 ±
190 50.7 nmol/min/mg, a K_M(CHS) of 0.80 mM, and a k_{cat} of 1.74 s^{-1} (**Figure 6 & Table 2**). The
191 catalytic rates of the mutants decreased by 70-90%, but except for G5-A540F, both G5-E146Q
192 and G8-R543S displayed significantly larger K_M(CHS), up to 200% increase. This suggests a

193 more profound impact of sitosterolemia mutations on the ABCG5/G8 ATPase activity through
194 sterol-protein interaction or structural changes.

195 ***Missense mutations cause conformational changes at the ATP-binding site.*** To examine the
196 relationship between structural changes of missense mutations and their impact on the ATPase
197 activity, we have performed molecular dynamics (MD) simulations for the WT and three mutants
198 in this study. We then analyzed the MD structures to understand how the mutations could lead to
199 different conformation around the hypothetical surrounding residues at the nucleotide-binding
200 sites (NBS). These residues were obtained through a structural comparison between the crystal
201 structure of ABCG5/G8 (PDB ID: 5DO7) and a cryo-EM structure of ABCG2 (PDB ID: 6HBU)
202 for which two ATP were bound in the homodimer (Lee et al., 2016; Manolaridis et al., 2018). In
203 this study, we have focused on the active nucleotide-binding site (known as NBS2) in
204 ABCG5/G8 (Lee et al., 2016) and analyzed residues 48-62, 68, 86-94, 134, 218, 250, 251, 267,
205 268, 302 of ABCG5 and 242-244 of ABCG8. As shown in **Figure 7**, the mutations at the three
206 sites can lead to global changes on the overall ABCG5/G8 structure, with values of root-mean-
207 square deviations (RMSDs) larger than 2.0 Å. The difference between the RMSDs of the
208 secondary structures is smaller, probably because more obvious changes need longer simulation
209 time to manifest. We are especially interested in the mutational effect on the ATP-binding site
210 and generated The RMSD *vs*. Simulation Time curves for those hypothetic surrounding residues
211 (**Supplementary Figure 2**). We observed that the RMSDs with and without least-square (LS)
212 fitting are very stable for the WT, whereas for G5-E146Q and G5-A540F, both the LS Fitting
213 and No-Fitting RMSD are significantly larger. However, G8-R543S mutation did not lead to
214 significantly larger RMSD, probably because the mutation effect needs longer simulation time to
215 reach the ATP-binding site. Indeed, the RMSD has a trend of getting large along the MD

216 simulation time for G8-R543S (**Supplementary Figure 2D**). Overall, we observed a significant
217 perturbation on the conformations of the putative surrounding residues due to the mutations at all
218 the three sites.

219 We then identified representative MD conformations for all four protein systems for
220 comparison (**Figure 8**). It is observed that three positively charged residues, K92, H49 and R50
221 of ABCG5 are overlaid very well between the crystal and MD structures for the WT (**Figure**
222 **8E**), while for the three mutants, at least one residue cannot be well-superimposed. Interestingly,
223 R52, another charged residue in ABCG5, is more distant from the center of the ATP-binding site.
224 Therefore, the conformational changes from our molecular modeling can qualitatively explain
225 why the three mutations can lead to impaired ATPase activity. Of particular note, the K92 is part
226 of the Walker A motif at the active nucleotide-binding site and required for ABCG5/G8
227 functions (Johnson et al., 2010; Zhang et al., 2006).

228 **DISCUSSION**

229 In this study, we have shown that CHS stimulates the ATPase activity of the human
230 ABCG5/G8 sterol transporter (**Figure 3**). The specific activity of ATP hydrolysis by ABCG5/G8
231 is by far the highest in comparison with the previously reported values (Johnson et al., 2010). In
232 contrast, when preincubated with sodium cholate and *E. coli* polar lipids, the purified G8-G216D
233 mutant displayed no ATPase activity, regardless of whether CHS is present or not. CHS is a
234 relatively water-soluble cholesterol analog and is used to mimic cholesterol in membrane protein
235 crystallization (Hanson et al., 2008; Lee et al., 2016). Our results showing CHS-stimulated
236 ATPase activity suggest that the sterol molecules may have played a role in promoting an active
237 conformation for the ATPase and/or enhancing the stability of ABCG5/G8. This idea of protein

238 stability is supported by recent findings showing that CHS stabilizes a variety of human
239 membrane proteins (Neumann et al., 2017). Our results herein provide the first biochemical
240 evidence of ABCG5/G8 functionality that is directly coupled with sterol substrates. The much
241 increased CHS-coupled ATPase activity indicates that ABCG5/G8 may need such a high ATP
242 catalytic rate to achieve the sterol-transport function across the cellular membranes.

243 We further demonstrated the stimulation of activity by CHS in a concentration-dependent
244 manner and increasing concentrations of ATP (**Figures 4, 5 & 6**). In the presence of *E. coli* polar
245 lipids, the catalytic rates were similar between the CHS and ATP-dependent ATPase activities, a
246 V_{max} of ~700 nmol/min/mg, which is about four times higher than that in the presence of liver
247 polar lipids (**Tables 1 & 2**) and more than two-fold higher than the previously reported value,
248 ~290 nmol/min/mg (Johnson et al., 2010). Using *E. coli* polar lipids, the K_M(ATP), 0.6 mM, is
249 about half of the previously reported 1 mM (Johnson et al., 2010), while in the presence of liver
250 polar lipids, K_M(ATP) remains ~1 mM (**Table 1**). In the current study, polar lipids, cholate (bile
251 acid) and CHS were also present in the reaction, indicating that the presence of *E. coli* polar
252 lipids results in higher ATP association and consequently better stimulates ABCG5/G8 ATPase
253 activity. When comparing the calculated values of k_{cat} and k_{cat}/K_M, we indeed observed an overall
254 5-fold higher turnover rate in the presence of *E. coli* polar lipids than liver polar lipids.

255 Interestingly, PE, the phospholipid found in both *E. coli* and liver lipids, is sufficient to
256 stimulate ATP hydrolysis in ABCG5/G8 to almost the highest activity, as reported in this study.
257 Using another phospholipid, PC or PG, alone, the specific activity of ABCG5/G8 was higher
258 than that obtained with the liver polar lipid mixture (**Figure 4**). PE is the major phospholipid of
259 the *E. coli* polar lipids, ~60%, and the second abundant phospholipid in the bile canalicular

260 membranes and the small intestine brush-border membranes, ~25% and ~40% respectively of
261 total phospholipids (Hauser et al., 1980; Kurumi et al., 1991). It has been shown that PE
262 preferentially fits the headgroup-binding sites on integral membrane proteins (Lee, 2004); thus,
263 PE may be recruited as better phospholipids to support ABCG5/G8 function in the cell
264 membranes. The approximate ratio of lipids for either *E. coli* or liver polar lipids may contribute
265 to the apparent difference in activity, but it remains unknown how phospholipid composition
266 regulates the transporter function. These individual lipids will be subjected to further
267 examination to define the lipid specificity on the ABCG5/G8 ATPase activity.

268 By mapping disease-carrying residues on the apo structure of ABCG5/G8, we have found
269 that most missense variants occur within or near the structural motifs consisting of several
270 conserved amino acids (Zein et al., 2019). Several missense mutations (ER-trapped) prevent
271 protein maturation from the endoplasmic reticulum (ER), but at least five mutations (ER-
272 escaped) have been shown to undergo proper trafficking to post-ER cell membranes (Graf et al.,
273 2004). So far, no report has shown the impact of these ER-escaped missense mutants on
274 ABCG5/G8 function using either *in vitro* or *in vivo* models. In this study, we have used purified
275 proteins from *Pichia pastoris* to investigate the functional activity of ABCG5/G8 *in vitro* and
276 aimed to establish the mechanistic basis of ABCG5/G8 through analyzing the structure-function
277 relationship of its loss-of-function missense mutations. The sitosterolemia missense mutants G5-
278 E146Q and G8-R543S have shown a reduction of CHS-coupled ATP hydrolysis, but retained
279 ~20% activity as compared to WT, while the putative sterol-binding mutant G5-A540F has
280 shown further reduction to ~10% of WT ATPase activity (**Figures 5 & 6**). With such activity
281 reduction, the mutant proteins maintained the ATPase activity similar to the basal level, as
282 shown by WT, suggesting a remote and allosteric regulation to keep ATPase active during the

283 reaction. As predicted by MD simulation, the ATP-bound homology model underwent global
284 conformational changes upon introducing the mutations (**Figure 7**). These mutations, albeit
285 relatively far away from the nucleotide-binding site, can cause significant structural
286 rearrangement of the residues within the region that encompass the active NBS2 (**Figure 8**).
287 Such conformational changes may alter responses to sterol-protein interaction necessary for
288 maximal ATPase activity.

289 In the atomic model of ABCG5/G8 (PDB ID: 5D07), G5-E146 is located on the E-helix
290 of the triple-helical bundle and in proximity to ABCG5's polar relay, while G8-R543 is part of
291 ABCG8's polar relay in the core of TMD (**Figure 1**). Both triple-helical bundle and polar relay
292 are believed to form a network of hydrogen bonding and salt bridges and play an important role
293 in inter-domain communication during the transporter function (Lee et al., 2016). G5-E146 and
294 G8-R543 are found in the proximity of the hydrogen-bond distance with Arginine 377 of
295 ABCG5 (G5-R377) and Glutamate 503 of ABCG8 (G8-503), respectively (**Figure 1B**). Based
296 on the ATP-dependent experiments (**Figure 5 & Table 1**), we obtained the changes of Gibbs
297 free energy from WT to each mutant ($\Delta\Delta G_{MUT}$) as $\Delta\Delta G_{E146Q}$ = ~11.7 kJ/mol and $\Delta\Delta G_{R543S}$ = ~12.3
298 kJ/mol. Such energetic loss is in the range of intramolecular hydrogen-bonding potential
299 observed on transmembrane a-helical bundles (Feldblum and Arkin, 2014). Therefore, the results
300 support the hypothesis that the E-helix and the polar relay are responsible for transmitting signals
301 between NBD and TMD. Slightly lower $\Delta\Delta G_{MUT}$ was observed from CHS-dependent
302 experiments (**Figure 6 & Table 2**), $\Delta\Delta G_{E146Q}$ = ~10.0 kcal/mol and $\Delta\Delta G_{R543S}$ = ~9.0 kcal/mol.
303 This falls in the range of hydrophobic interaction and argues weakened sterol-transporter
304 interaction due to these disease mutations. As for the sterol-binding mutant, we obtained higher
305 energetic loss, but similar $\Delta\Delta G_{MUT}$ from ATP- or CHS-dependent analysis, $\Delta\Delta G_{A540F}$ = ~15.8 or

306 ~16.1 kJ/mol, respectively. This likely indicates a strong hydrophobic interaction between sterols
307 and the transporter, as no obvious hydrogen donors/acceptors can be found at the putative sterol-
308 binding site on the crystal structure. In addition, G5-A540 is distant from the polar relay (>10Å
309 away); thus, this data suggests a remote contact by sterol molecules to control the sterol-coupled
310 signaling, likely through the polar relay in the transmembrane domains. In the ATP
311 concentration-dependent experiments, the K_M values for ATP remained almost the same (**Table**
312 **1**), suggesting that ATP binding was not affected by these mutants. The K_M values for CHS was
313 significantly increased in the disease mutants, but not the sterol-binding mutant (**Table 2**),
314 suggesting that CHS interacts with ABCG5/G8 and remotely regulates the turnover of ATP
315 hydrolysis in either sequential (Mode 1) or concerted (Mode 2) pathway (**Figure 9**).
316 Collectively, these results argue that a working network of E-helix and polar relay is essential to
317 maintain the communication between ATPase and sterol-binding activities in ABCG5/G8, which
318 are impaired by the loss-of-function missense mutations.

319 In conclusion, these studies show that CHS stimulates ABCG5/G8 ATPase activity and
320 may promote an active conformation for ABCG5/G8-mediated sterol transport. The enzymatic
321 characterization of three loss-of-function missense variants provides a mechanistic basis of how
322 the polar relay contributes to the inter-domain communication for the sterol-coupled ATPase
323 activity in ABCG5/G8 and may be directly involved in such ligand-protein interactions. Further
324 studies will reveal more insight into these molecular events and enable sterol-lowering
325 therapeutics to treat sitosterolemia and hypercholesterolemia.

326

327 **MATERIALS AND METHODS**

328 **Materials.** *E. coli* polar lipids (Cat. #: 100600C) and bovine liver polar lipids (Cat. #: 181108C)
329 were from Avanti Polar Lipids, Inc. (via MilliporeSigma). Cholesterol, cholesteryl hemisuccinate
330 (CHS), and n-Dodecyl β-D-maltopyranoside (DDM) were from Anatrace. The Ni-NTA agarose
331 resin was from Qiagen, the calmodulin (CBP) affinity resin, zeocin, and ampicillin were from
332 Agilent. Imidazole, ε-aminocaproic acid, sucrose, yeast extract, tryptone, peptone, yeast nitrogen
333 base (YNB), and ammonium sulfate were obtained from Wisent. ATP disodium trihydrate, Tris-
334 (2-carboxyethyl)-phosphine (TCEP), sodium chloride, glycerol, ethylene diamine-tetraacetic acid
335 (EDTA), ethylene glycol-bis(□-aminoethyl ether)-N,N,N',N'-tetraacetic acid (EGTA), sodium
336 dodecyl sulfate (SDS), Ponceau S solution, sodium azide, Bradford reagents, Tween 20,
337 magnesium chloride, calcium chloride, and all protease inhibitors were obtained from Bioshop
338 Canada. Biotin, sodium cholate hydrate, L-ascorbic acid, ammonium molybdate, bismuth citrate,
339 sodium citrate, methanol, ammonium hydroxide, hydrochloric acid, and acetic acid were
340 obtained from MilliporeSigma. Dithiothreitol (DTT), Tris base and Tris acetate were obtained
341 from ThermoFisher. Clarity Western ECL substrates, 30 % acrylamide, agarose and ammonium
342 persulfates were obtained from Bio-Rad. Restriction enzymes were obtained from New England
343 Biolabs, Promega and ThermoFisher. YPD: Yeast extract Peptone Dextrose; YPDS: Yeast
344 extract Peptone Dextrose Sorbitol; MGY: Minimal Glycerol Yeast nitrogen base; mPIB
345 (minimal protease inhibitor buffer for yeast cell lysis): 0.33 M sucrose, 0.3 M Tris-HCl (pH 7.5),
346 1 mM EDTA, 1mM EGTA, and 100mM ε-aminocaproic acid, ddH_2O to a final volume of 1 L
347 and stored at 4°C.

348 **Cloning of ABCG5/G8 missense mutants.** The expression vectors (pLIC and pSGP18),
349 carrying human ABCG5 (NCBI accession number NM_022436) and human ABCG8 (NCBI
350 accession number NM_022437), were derived from pPICZB (Invitrogen) as described (Johnson
351 et al., 2010; Wang et al., 2006), pLIC-ABCG5 and pSGP18-ABCG8, respectively. A tandem
352 array of six histidines separated by glycine ($His_6GlyHis_6$) was added to the C terminus of
353 ABCG5, and A tag encoding a rhinovirus 3C protease site followed by a calmodulin binding
354 peptide (CBP) was added to the C terminus of ABCG8. To generate the missense mutants in this
355 study, we performed site-directed mutagenesis by using WT ABCG5 or ABCG8 as the templates
356 and the following codon-optimized oligonucleotide primers (Eurofins Genomics Canada). G5-
357 A540F: CCATTTTTGGGGTGCTTGTTGGATCTGGATTCCTCAG (forward) and
358 GCACCCCAAAAATGGACAGCAGAGCCACTACAC (reverse); G5-E146Q:
359 GCGCCAAACGCTGCACTACACCGCGCTGC (forward) and
360 CAGCGTTTGGCGCACGGTGAGGCTGCTCAG (reverse); G8-R543S:
361 GTTGCTCTATTATGGCCCTGGCCGCCGC (forward) and
362 GCCATAATAGAGCAACAGAAGACCACCAGCCAC (reverse); G8-G216D:
363 ACGAGCGCAGGAGAGTCAGCATTGGGGTGCAG (forward) and
364 CTCTCCTGCGCTCGTCCCCCGACAACCCC (reverse). The polymerase chain reaction (PCR)
365 included 1-unit Phusion High-Fidelity DNA Polymerase (New England Biolabs), 1x Phusion
366 buffer, 200 mM dNTP, 2% (v/v) DMSO, 100 ng DNA templates, and 0.4 mM forward and
367 reverse primers. Each mutant-containing plasmid was amplified by the following PCR setting:
368 initial DNA denaturation (98°C, 2 minutes), followed by 30 cycles of denaturation (98°C, 15
369 seconds) / primer annealing (55°C, 30 seconds) / DNA extension (72°C, 3 minutes), then final
370 extension (72°C, 20 minutes). 5μl of the PCR products was run on a 1% agarose gel to confirm

371 the amplification, and 1µl of Dnp1 restriction enzymes (20 units) was used to digest the WT
372 templates overnight at 37°C to. The modified plasmids were cleaned up by ethanol acetate
373 precipitation technique. 5µl of 3M Sodium acetate was added to each 50µl PCR product. 200µl
374 of 100% Ethanol was added to each tube, vortexed, and left at room temperature for 10 minutes.
375 At max speed in a table centrifuge for 10 minute the plasmids were pelleted the supernatant was
376 removed then washed by 75% ethanol. Residual ethanol was dried by a Speed-Vac at the
377 maximal speed for 20 minutes at room temperature. The pellet was resuspended in ddH_2O.
378 Mutants plasmids were cloned into XL1-Blue competent *E. coli* cells by the heat-shock approach
379 as described in the supplier's manual (Novagen/Agilent) and by antibiotic selection using Zeocin
380 (Invitrogen/ThermoFisher). Using PureYield Plasmid Midiprep kit (Promega), DNA
381 preparations of selected clones were subjected to sequencing at Eurofins Genomics Canada.

382 **Expression of ABCG5/G8 missense mutants in *Pichia pastoris* yeast (Supplementary Figure**
383 **1A).** Both WT and mutant plasmids (20 mg each plasmid) were linearized using PmeI and co-
384 transformed into the *Pichia* strain KM71H by electroporation. Immediately the cells were
385 resuspended with 1-mL ice cold 1M sorbitol and incubated at 30°C for 1 hour. Then 5mL fresh
386 YPD were added and incubated for 6 hours at 250 rpm and 30°C. The cells were then centrifuged
387 at 3000xg for 10 minutes and resuspended with 200µL of YPD. 100 µL of transformants were
388 plated on YPDS plates containing 100 (low), 500 (medium) or 1000 (high) µg/mL of Zeocin to
389 screen for successful transformation. Seven colonies were picked and grown in 10 mL of MGY
390 media for 24 hours in sterile 50 mL tubes at 250 rpm and 30°C. The cells were centrifuged for 10
391 minutes at 3000xg and the resuspended with 10 mL of MM media. 50 µL methanol was added to
392 the media and once again after 12 hours. The cells were harvested after 24-hour incubation at
393 250 rpm and 30°C, resuspended in 600 µL mPIB buffer transferred into 1.5 mL Eppendorf tube.

394 After adding 500 μL glass bead, protease inhibitors, and 10mM DTT, the cells were lysed using
395 a mini-bead beater (Biospec), 1.5 minutes beating and 1.5 minutes rest on ice for 3 cycles. The
396 unbroken cells and beads were pelleted by centrifugation at 5000×g for 5 minutes at 4°C,
397 followed by 21130xg for 5 minutes at 4°C. The supernatant was collected, and the concentration
398 of the total proteins was estimated by Bradford assay. 1 µl of cell lysate alongside a 0 µg to 10
399 µg BSA standards were each added to a 200 µl Bradford reagent on a 96-well plate. Absorbance
400 at 595 nm was used to measure the protein concentrations using a Synergy H1 Hybrid reader.
401 The cell lysates (20 or 30 µg of total proteins) was resolved by SDS–PAGE, and protein
402 expression was analyzed by immunoblotting using monoclonal anti-RGSH4 antibodies (Qiagen)
403 to detect ABCG5 and polyclonal anti-hABCG8 antibodies (Novus Biologicals) to detect
404 ABCG8. The clones expressing the highest level for both subunits were selected and stored in
405 20% glycerol at -75°C.

406 **Cell culture and microsomal membrane preparation.** The conditions for cell growth and WT
407 protein induction were as described (14). Briefly, cells were initially grown at 30°C to
408 accumulate cell mass in an Innova R43 shaker (Eppendorf) at 250 rpm for 24-48 hours with the
409 pH maintained at pH 5-6. To induce protein expression, cells were left fasting for 6-12 hours,
410 then incubated with 0.1% (v/v) methanol for 6–12 hours at 20 or 28°C. The methanol
411 concentration was increased to 0.5% (v/v) by adding methanol every 12 hours for 48-60 hours.
412 Cell pellets were collected and resuspended in mPIB and stored at -75°C. Approximately 45 ± 10
413 g of cell mass was typically obtained from 1 L of cultured cells. The frozen cells were thawed
414 and lysed using a C3-Emulsifier (Avestin) in mPIB in the presence of 10 mM DTT and protease
415 inhibitors (1 µg/ml leupeptin, 1 µg/ml pepstatin A, 1 µg/ml aprotinin, and 2 mM PMSF). The
416 microsomal membranes were then prepared, as described (Lee et al., 2016).

417 **Purification of ABCG5/G8 and its mutants.** Both WT and mutants were purified following a
418 protocol as described previously (Lee et al., 2016), with minor modification. Briefly, DDM-
419 solubilized membranes were subjected to a tandem affinity column chromatography, first using
420 Ni-NTA and then CBP. The N-linked glycans and the CBP tag remained on the purified
421 heterodimers, and the CBP eluates were further purified by gel-filtration chromatography using a
422 Superdex 200 Increase 10/300 GL column on an ÄKTA Pure purification system (Cytiva,
423 formerly GE Healthcare Life Sciences). The proteins in the peak fractions were collected and
424 concentrated to 1-3 mg/mL for storage at -75°C. Noticeably, the final yield for mutants was
425 lower than WT, in a range of 400-800μg per six liters of cells. The expression level of the mutant
426 proteins in the microsomes and their solubility was slightly lower than WT. Some proteins were
427 also lost during Ni-NTA binding and imidazole wash. The profile of the gel-filtration
428 chromatography often showed a higher peak at the void volume than dimeric proteins. These
429 factors collectively suggest that the mutant proteins are more prone to aggregation, and thus
430 explain the lower yields.

431 **ATPase assay.** We have consistently observed a strong cloudiness in the assay solution when
432 using previous protocols, consequently resulting in low sensitivity of detecting the ABCG5/G8
433 ATPase activity. Because a high concentration of bile acids is required, we have reasoned that
434 the high content of detergents, both in the assay solution and in the protein preparations, may
435 have caused either high background upon quenching the reaction in the Malachite Green-based
436 assay (Johnson et al., 2010) or poor organic-aqueous phase separation (Lee et al., 2016). The
437 measurement of ATPase activity has thus become inconsistent from one protein preparation to
438 another. To overcome this issue, we first optimized the ATPase assay by adopting a colorimetric
439 and bismuth citrate-based approach (Cariani et al., 2004), which also allows high-throughput

440 detection of the liberated inorganic phosphate by a microplate reader. The ATPase assay was
441 performed in a 65μl final reaction volume containing 2mg/ml *E. coli* or liver polar lipids or
442 designated phospholipids, 1.5% sodium cholate, 0.2% (4.11mM) CHS, and 2mM DTT in Buffer
443 A (50mM Tris/Cl pH 7.5, 100mM NaCl, 10% glycerol, 0.1% DDM). The Lipid/CHS/DTT
444 mixture was thoroughly sonicated and preincubated with ABCG5/G8 proteins (0.3 to 1.5 μg) for
445 5 minutes at room temperature. The catalytically deficient G8-G216D was used as the negative
446 control.

447 The enzymatic activity of ABCG5/G8 was initiated upon the addition of the 10X ATP cocktail
448 (6.5μl) and incubated at 37°C. Aliquots (8.5μl) were removed every 2 minutes and added to the
449 pre-chilled quencher wells to stop the reaction. The quencher solution was made of 5% SDS in
450 5mM HCl. Lipid mixtures were prepared at 30mg/ml (~20mM) in Buffer A containing 7%
451 sodium cholate. CHS stock solution (1%, w/v) was prepared in a Buffer A and 4.5% sodium
452 cholate. 10X Mg/ATP cocktail contains 50mM ATP, 75mM $MgCl_2$, 100mM NaN_3 in a buffer
453 containing 50mM Tris/Cl pH 7.5. To detect the liberated inorganic phosphate, 50μL of freshly-
454 made Solution II (142mM ascorbic acid, 0.42M HCl, 4.2% Solution I (10% ammonium
455 molybdate) was added to plate wells and left on ice for 10 minutes. Then 75μl Solution III
456 (88mM bismuth citrate, 120mM sodium citrate, 1M HCl) was added to plate wells and placed at
457 37°C for 10 minutes. The absorbance was measured at 695nm using a multi-well plate reader.
458 For the phosphate standards, 1M monobasic or dibasic sodium or potassium phosphate in 50mM
459 Tris/Cl pH 7.5 was prepared, and six standard inorganic phosphate solutions (0μM, 12.5μM,
460 25μM, 50μM, 100μM, 200μM) were used in every experiment. The linear range of each reaction
461 was used to calculate the initial rate of ATP hydrolysis. GraphPad Prism 8 was used to perform
462 nonlinear regression and ordinary one-way ANOVA, with a P value of ≤0.05 considered

463 significant from at least three independent experiments. The kinetic parameters were calculated
464 by nonlinear Michaelis-Menten curve fitting using GraphPad Prism 8.

465 **Computational Methods.** We studied four ABCG5/G8 protein systems including the WT,
466 E146Q, A540F and R543S mutants. Each MD system consists of one copy of ABCG5/G8
467 heterodimer, 320 1,2-Dimyristoyl-sn-glycero-3-phosphocholine (DMPC) lipid, 16 Cholesterol,
468 43,621 TIP3P (Jorgensen et al., 1983) water molecules, 103 Cl^- and 83 Na^+ to neutralize the MD
469 systems. AMBER ff14SB (Maier et al., 2015), Lipid14 (Dickson et al., 2014) and GAFF (Wang
470 et al., 2004) force fields were used to model proteins, DMPC lipids and Cholesterols,
471 respectively. The residue topology of cholesterol was prepared using the Antechamber module
472 (Dickson et al., 2014). MD simulation was performed to produce isothermal-isobaric ensembles
473 using the pmemd.cuda program in AMBER 18 (Case et al., 2018). The Particle Mesh Ewald
474 (PME) method (Darden et al., 1999) was used to accurately calculate the electrostatic energies
475 with the long-ranged correction taken into account. All bonds were constrained using the
476 SHAKE algorithm (Miyamoto and Kollman, 1992) in both the minimization and MD simulation
477 stages following a computational protocol described in our previous publication (Lee et al.,
478 2016). Briefly, there were three stages in a series of constant pressure and temperature MD
479 simulations, including the relaxation phase, the equilibrium phase, and the sampling phase. In the
480 relaxation phase, the simulation system was heated up progressively from 50K to 250K at steps
481 of 50K and 1-nanosecond MD simulation was run at each temperature. In the next equilibrium
482 phase, the system was equilibrated at 298K, 1 bar for 10 ns. Finally, a 100-nanosecond MD
483 simulation was performed at 298K, 1 bar to produce isothermal–isobaric ensemble ensembles. In
484 total, 1,000 snapshots were recorded from the last phase simulation for post-analysis using
485 “cpptray” module implement in the AMBER software package.

ACKNOWLEDGMENTS

We thank William Jennings, Gloria Ihirwe, Midhet Hajira and Chloé van de Panne for technical assistance. We also thank Donna Clary and Hui Li for their technical help in utilizing the common core facilities. We are indebted to critical feedback on reviewing the manuscript from Ms. Vicky Brandt, and Drs. John Baenziger, Jean-François Couture, Gregory Graf and Xiaohui Zha. This work is partially based on the theses that were submitted to fulfill in part the requirement for the degrees of Master of Science (A.A.Z.) and Honors Bachelor of Science (A.V.).

AUTHOR CONTRIBUTIONS

B.M.X. optimized the CHS-stimulated ATPase assay for ABCG5/G8; A.A.Z. generated and validated the mutant constructs; B.M.X., A.A.Z. and A.V. purified the proteins and carried out the ATPase assays and data analysis. J.W. performed the molecular dynamics simulation, J.-Y.L. oversaw the project, and J.W. and J.-Y.L. wrote the manuscript. All authors have read and agreed to the submitted version of the manuscript.

FUNDING

This research was funded by a startup grant from the University of Ottawa, a Discovery Grant from the Natural Sciences and Engineering Research Council (RGPIN 2018-04070), and a National New Investigator Award from the Heart and Stroke Foundation of Canada to J.-Y.L. and the National Institutes of Health grants (R01-GM079383 and R21-GM097617) to J.W. B.M.X. is a recipient of the Travel Awards from the Canadian Society of Molecular Biosciences (2018) and Biophysical Society of Canada (2019).

CONFLICT OF INTEREST

The authors declare no conflict of interest. The funders had no role in the design of the study; in the collection, analyses, or interpretation of data; in the writing of the manuscript, or in the decision to publish the results.

512 **ABBREVIATIONS**

ABC	ATP-binding cassette
ABCC7	ATP-binding cassette sub-family C member 7
ABCG5	ATP-binding cassette sub-family G member 5
ABCG8	ATP-binding cassette sub-family G member 8
ATP	Adenosine triphosphate
CBP	Calmodulin-binding peptide
CFTR	Cystic fibrosis transmembrane conductance regulator
CHS	Cholesteryl hemisuccinate
DDM	Dodecyl maltoside or n-Dodecyl β-D-maltopyranoside
DMPC	1,2-Dimyristoyl-sn-glycero-3-phosphocholine
DNA	Deoxyribonucleic acid
DTT	Dithiothreitol
EDTA	Ethylene diamine-tetraacetic acid
EGTA	Ethylene glycol-bis(□-aminoethyl ether)-N,N,N',N'-tetraacetic acid
ER	Endoplasmic reticulum
ICL	Intracellular loop
LDL	Low-density lipoprotein
LOF	Loss of function
LS	Least square
MD	Molecular dynamics
MGY	Minimal glycerol yeast nitrogen base
MM	Minimal methanol
mPIB	Minimum protease inhibitor buffer
NBD	Nucleotide-binding domain
NBS	Nucleotide-binding site
Ni-NTA	Nickle-nitrilotriacetic acid
PC	Phosphatidylcholine
PCR	Polymerase chain reaction
PDB	Protein data bank
PE	Phosphatidylethanolamine
PG	Phosphatidylglycerol
RCT	Reverse cholesterol transport
RMSD	Root mean square deviation
SDS	Sodium dodecyl sulfate
TCEP	Tris-(2-carboxyethyl)-phosphine
TICE	Transintestinal cholesterol efflux
TMD	Transmembrane domain
WT	Wild type
YNB	Yeast nitrogen base
YPD	Yeast extract peptone dextrose
YPDS	Yeast extract peptone dextrose sorbitol

513

514 **REFERENCES**

515 Berge KE, Tian H, Graf GA, Yu L, Grishin N V., Schultz J, Kwiterovich P, Shan B, Barnes R,
516 Hobbs HH. 2000. Accumulation of dietary cholesterol in sitosterolemia caused by
517 mutations in adjacent ABC transporters. *Science (80-)* **290**:1771–1775.
518 doi:10.1126/science.290.5497.1771

519 Bhattacharyya AK, Connor WE, Lin DS, McMurry MM, Shulman RS. 1991. Sluggish sitosterol
520 turnover and hepatic failure to excrete sitosterol into bile cause expansion of body pool of
521 sitosterol in patients with sitosterolemia and xanthomatosis. *Arterioscler Thromb* **11**:1287–
522 1294. doi:10.1161/01.atv.11.5.1287

523 Borst P, Zelcer N, Van Helvoort A. 2000. ABC transporters in lipid transport. *Biochim Biophys*
524 *Acta - Mol Cell Biol Lipids* **1486**:128–144. doi:10.1016/S1388-1981(00)00053-6

525 Buch S, Schafmayer C, Völzke H, Becker C, Franke A, Von Eller-Eberstein H, Kluck C,
526 Bässmann I, Brosch M, Lammert F, Miquel JF, Nervi F, Wittig M, Rosskopf D, Timm B,
527 Höll C, Seeger M, Elsharawy A, Lu T, Egberts J, Fändrich F, Fölsch UR, Krawczak M,
528 Schreiber S, Nürnberg P, Tepel J, Hampe J. 2007. A genome-wide association scan
529 identifies the hepatic cholesterol transporter ABCG8 as a susceptibility factor for human
530 gallstone disease. *Nat Genet* **39**:995–999. doi:10.1038/ng2101

531 Cariani L, Thomas L, Brito J, Del Castillo JR. 2004. Bismuth citrate in the quantification of
532 inorganic phosphate and its utility in the determination of membrane-bound phosphatases.
533 *Anal Biochem* **324**:79–83. doi:10.1016/j.ab.2003.09.008

534 Case DA, Ben-Shalom IY, Brozell SR, Cerutti DS, Cheatham III TE, Cruzeiro VWD, Darden
535 TA, Duke RE, Ghoreishi D, Gilson MK. 2018. Amber 2018; 2018, University of California,
536 San Francisco.

537 Chen ZC, Shin SJ, Kuo KK, Lin K Der, Yu ML, Hsiao PJ. 2008. Significant association of
538 ABCG8:D19H gene polymorphism with hypercholesterolemia and insulin resistance. *J*
539 *Hum Genet* **53**:757–763. doi:10.1007/s10038-008-0310-2

540 Darden T, Perera L, Li L, Lee P. 1999. New tricks for modelers from the crystallography toolkit:
541 The particle mesh Ewald algorithm and its use in nucleic acid simulations. *Structure* **7**:R55–
542 R60. doi:10.1016/S0969-2126(99)80033-1

543 Davies DR, Hol WGJ. 2004. The power of vanadate in crystallographic investigations of
544 phosphoryl transfer enzymes. *FEBS Lett* **577**:315–321. doi:10.1016/j.febslet.2004.10.022

545 Dean M, Allikmets R. 1995. Evolution of ATP-binding cassette transporter genes. *Curr Opin*
546 *Genet Dev* **5**:779–785. doi:10.1016/0959-437X(95)80011-S

547 Dean M, Hamon Y, Chimini G. 2001. The human ATP-binding cassette (ABC) transporter
548 superfamily. *J Lipid Res* **42**:1007–1017. doi:10.1101/gr.184901

549 Dickson CJ, Madej BD, Skjevik ÅA, Betz RM, Teigen K, Gould IR, Walker RC. 2014. Lipid14:
550 The amber lipid force field. *J Chem Theory Comput* **10**:865–879. doi:10.1021/ct4010307

551 Feldblum ES, Arkin IT. 2014. Strength of a bifurcated H bond. *Proc Natl Acad Sci U S A*
552 **111**:4085–4090. doi:10.1073/pnas.1319827111

553 Ford RC, Beis K. 2019. Learning the ABCs one at a time: Structure and mechanism of ABC

554 transporters. *Biochem Soc Trans* **47**:23–36. doi:10.1042/BST20180147

555 Graf GA, Cohen JC, Hobbs HH. 2004. Missense mutations in ABCG5 and ABCG8 disrupt
556 heterodimerization and trafficking. *J Biol Chem* **279**:24881–24888.
557 doi:10.1074/jbc.M402634200

558 Graf GA, Li W-P, Gerard RD, Gelissen I, White A, Cohen JC, Hobbs HH. 2002. Coexpression
559 of ATP-binding cassette proteins ABCG5 and ABCG8 permits their transport to the apical
560 surface. *J Clin Invest* **110**:659–669. doi:10.1172/jci16000

561 Graf GA, Yu L, Li WP, Gerard R, Tuma PL, Cohen JC, Hobbs HH. 2003. ABCG5 and ABCG8
562 Are Obligate Heterodimers for Protein Trafficking and Biliary Cholesterol Excretion. *J Biol*
563 *Chem* **278**:48275–48282. doi:10.1074/jbc.M310223200

564 Hanson MA, Cherezov V, Griffith MT, Roth CB, Jaakola VP, Chien EYT, Velasquez J, Kuhn P,
565 Stevens RC. 2008. A Specific Cholesterol Binding Site Is Established by the 2.8 Å
566 Structure of the Human β2-Adrenergic Receptor. *Structure* **16**:897–905.
567 doi:10.1016/j.str.2008.05.001

568 Hauser H, Howell K, Dawson RMC, Bowyer DE. 1980. Rabbit small intestinal brush border
569 membrane. Preparation and lipid composition. *Biochim Biophys Acta - Biomembr* **602**:567–
570 577. doi:10.1016/0005-2736(80)90335-1

571 Hirayama H, Kimura Y, Kioka N, Matsuo M, Ueda K. 2013. ATPase activity of human ABCG1
572 is stimulated by cholesterol and sphingomyelin. *J Lipid Res* **54**:496–502.
573 doi:10.1194/jlr.M033209

574 Hwang JU, Song WY, Hong D, Ko D, Yamaoka Y, Jang S, Yim S, Lee E, Khare D, Kim K,
575 Palmgren M, Yoon HS, Martinoia E, Lee Y. 2016. Plant ABC Transporters Enable Many
576 Unique Aspects of a Terrestrial Plant's Lifestyle. *Mol Plant* **9**:338–355.
577 doi:10.1016/j.molp.2016.02.003

578 Jakulj L, van Dijk TH, de Boer JF, Kootte RS, Schonewille M, Paalvast Y, Boer T, Bloks VW,
579 Boverhof R, Nieuwdorp M, Beuers UHW, Stroes ESG, Groen AK. 2016. Transintestinal
580 Cholesterol Transport Is Active in Mice and Humans and Controls Ezetimibe-Induced Fecal
581 Neutral Sterol Excretion. *Cell Metab* **24**:783–794. doi:10.1016/j.cmet.2016.10.001

582 Johnson BJH, Lee JY, Pickert A, Urbatsch IL. 2010. Bile acids stimulate atp hydrolysis in the
583 purified cholesterol transporter ABCG5/G8. *Biochemistry* **49**:3403–3411.
584 doi:10.1021/bi902064g

585 Jorgensen WL, Chandrasekhar J, Madura JD, Impey RW, Klein ML. 1983. Comparison of
586 simple potential functions for simulating liquid water. *J Chem Phys* **79**:926–935.
587 doi:10.1063/1.445869

588 Kajinami K, Brousseau ME, Ordovas JM, Schaefer EJ. 2004. Interactions between common
589 genetic polymorphisms in ABCG5/G8 and CYP7A1 on LDL cholesterol-lowering response
590 to atorvastatin. *Atherosclerosis* **175**:287–293. doi:10.1016/j.atherosclerosis.2004.03.015

591 Kizhakkedath P, John A, Al-Sawafi BK, Al-Gazali L, Ali BR. 2019. Endoplasmic reticulum
592 quality control of LDLR variants associated with familial hypercholesterolemia. *FEBS*
593 *Open Bio* **9**:1994–2005. doi:10.1002/2211-5463.12740

594 Klett EL, Lu K, Kosters A, Vink E, Lee MH, Altenburg M, Shefer S, Batta AK, Yu H, Chen J,

595 Klein R, Looije N, Oude-Elferink R, Groen AK, Maeda N, Salen G, Patel SB. 2004. A
596 mouse model of sitosterolemia: Absence of Abcg8/sterolin-2 results in failure to secrete
597 biliary cholesterol. *BMC Med* **2**:5. doi:10.1186/1741-7015-2-5

598 Kuo KK, Shin SJ, Chen ZC, Yang YHC, Yang JF, Hsiao PJ. 2008. Significant association of
599 ABCG5 604Q and ABCG8 D19H polymorphisms with gallstone disease. *Br J Surg*
600 **95**:1005–1011. doi:10.1002/bjs.6178

601 Kurumi Y, Adachi Y, Itoh T, Kobayashi H, Nanno T, Yamamoto T. 1991. Novel high-
602 performance liquid chromatography for determination of membrane phospholipid
603 composition of rat hepatocytes. *Gastroenterol Jpn* **26**:628–632. doi:10.1007/BF02781680

604 Lee AG. 2004. How lipids affect the activities of integral membrane proteins. *Biochim Biophys*
605 *Acta - Biomembr* **1666**:62–87. doi:10.1016/j.bbamem.2004.05.012

606 Lee JY, Kinch LN, Borek DM, Wang Jin, Wang Junmei, Urbatsch IL, Xie XS, Grishin N V.,
607 Cohen JC, Otwinowski Z, Hobbs HH, Rosenbaum DM. 2016. Crystal structure of the
608 human sterol transporter ABCG5/ABCG8. *Nature* **533**:561–564. doi:10.1038/nature17666

609 Li G, Gu HM, Zhang DW. 2013. ATP-binding cassette transporters and cholesterol
610 translocation. *IUBMB Life* **65**:505–512. doi:10.1002/iub.1165

611 Linton KJ, Higgins CF. 1998. The Escherichia coli ATP-binding cassette (ABC) proteins. *Mol*
612 *Microbiol* **28**:5–13. doi:10.1046/j.1365-2958.1998.00764.x

613 Lu K, Lee MH, Hazard S, Brooks-Wilson A, Hidaka H, Kojima H, Ose L, Stalenhoef AFH,
614 Mietinnen T, Bjorkhem I, Bruckert E, Pandya A, Brewer HB, Salen G, Dean M, Srivastava

615 A, Patel SB. 2001. Two genes that map to the STSL locus cause sitosterolemia: Genomic
616 structure and spectrum of mutations involving sterolin-1 and sterolin-2, encoded by ABCG5
617 and ABCG8, respectively. *Am J Hum Genet* **69**:278–290. doi:10.1086/321294

618 Lukacs GL, Mohamed A, Kartner N, Chang XB, Riordan JR, Grinstein S. 1994. Conformational
619 maturation of CFTR but not its mutant counterpart (ΔF508) occurs in the endoplasmic
620 reticulum and requires ATP. *EMBO J* **13**:6076–6086. doi:10.1002/j.1460-
621 2075.1994.tb06954.x

622 Maier JA, Martinez C, Kasavajhala K, Wickstrom L, Hauser KE, Simmerling C. 2015. ff14SB:
623 Improving the Accuracy of Protein Side Chain and Backbone Parameters from ff99SB. *J*
624 *Chem Theory Comput* **11**:3696–3713. doi:10.1021/acs.jctc.5b00255

625 Manolaridis I, Jackson SM, Taylor NMI, Kowal J, Stahlberg H, Locher KP. 2018. Cryo-EM
626 structures of a human ABCG2 mutant trapped in ATP-bound and substrate-bound states.
627 *Nature* **563**:426–430. doi:10.1038/s41586-018-0680-3

628 Miyamoto S, Kollman PA. 1992. Settle: An analytical version of the SHAKE and RATTLE
629 algorithm for rigid water models. *J Comput Chem* **13**:952–962. doi:10.1002/jcc.540130805

630 Neumann J, Rose-Sperling D, Hellmich UA. 2017. Diverse relations between ABC transporters
631 and lipids: An overview. *Biochim Biophys Acta - Biomembr* **1859**:605–618.
632 doi:10.1016/j.bbamem.2016.09.023

633 Patel SB, Graf GA, Temel RE. 2018. ABCG5 and ABCG8: more than a defense against
634 xenosterols. *J Lipid Res* **59**:1103–1113. doi:10.1194/jlr.R084244

635 Plösch T, Bloks VW, Terasawa Y, Berdy S, Siegler K, Van Der Sluijs F, Kema IP, Groen AK,
636 Shan B, Kuipers F, Schwartz M. 2004. Sitosterolemia in ABC-Transporter G5-Deficient
637 Mice Is Aggravated on Activation of the Liver-X Receptor. *Gastroenterology* **126**:290–300.
638 doi:10.1053/j.gastro.2003.10.074

639 Takahashi K, Kimura Y, Kioka N, Matsuo M, Ueda K. 2006. Purification and ATPase activity of
640 human ABCA1. *J Biol Chem* **281**:10760–10768. doi:10.1074/jbc.M513783200

641 Wang J, Grishin N, Kinch L, Cohen JC, Hobbs HH, Xie XS. 2011. Sequences in the
642 nonconsensus nucleotide-binding domain of ABCG5/ABCG8 required for sterol transport. *J*
643 *Biol Chem* **286**:7308–7314. doi:10.1074/jbc.M110.210880

644 Wang J, Wolf RM, Caldwell JW, Kollman PA, Case DA. 2004. Development and testing of a
645 general Amber force field. *J Comput Chem* **25**:1157–1174. doi:10.1002/jcc.20035

646 Wang Z, Stalcup LD, Harvey BJ, Weber J, Chloupkova M, Dumont ME, Dean M, Urbatsch IL.
647 2006. Purification and ATP hydrolysis of the putative cholesterol transporters ABCG5 and
648 ABCG8. *Biochemistry* **45**:9929–9939. doi:10.1021/bi0608055

649 Xavier BM, Jennings WJ, Zein AA, Wang J, Lee JY. 2019. Structural snapshot of the
650 cholesterol-transport ATP-binding cassette proteins. *Biochem Cell Biol* **97**:224–233.
651 doi:10.1139/bcb-2018-0151

652 Yu L, Hammer RE, Li-Hawkins J, Von Bergmann K, Lutjohann D, Cohen JC, Hobbs HH. 2002.
653 Disruption of Abcg5 and Abcg8 in mice reveals their crucial role in biliary cholesterol
654 secretion. *Proc Natl Acad Sci U S A* **99**:16237–16242. doi:10.1073/pnas.252582399

655 Zein AA, Kaur R, Hussein TOK, Graf GA, Lee JY. 2019. ABCG5/G8: A structural view to
656 pathophysiology of the hepatobiliary cholesterol secretion. *Biochem Soc Trans* **47**:1259–
657 1268. doi:10.1042/BST20190130

658 Zhang DW, Graf GA, Gerard RD, Cohen JC, Hobbs HH. 2006. Functional asymmetry of
659 nucleotide-binding domains in ABCG5 and ABCG8. *J Biol Chem* **281**:4507–4516.
660 doi:10.1074/jbc.M512277200

661

662 **FIGURES AND TABLES.**

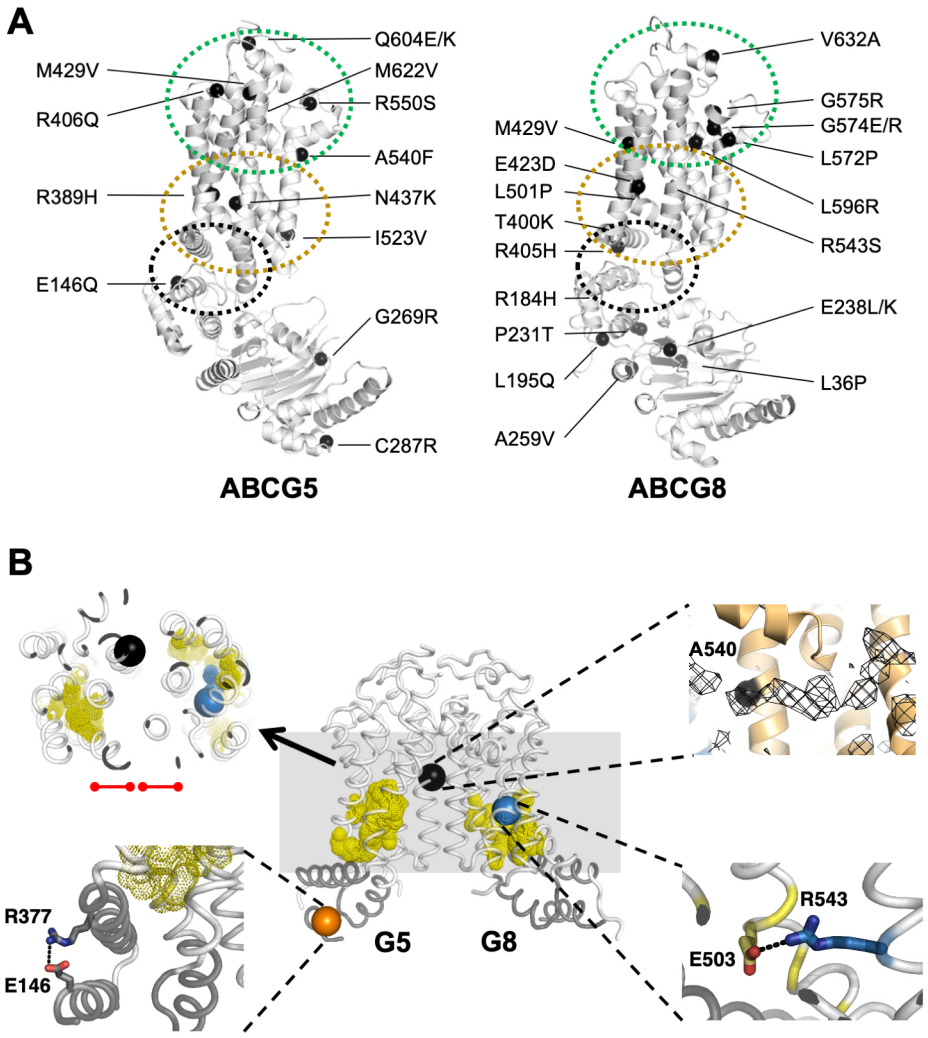

663

664

665 **Figure 1. Disease-causing mutations and SNPs in ABCG5/G8. A,** Localization of ABCG5/G8
666 residues carrying missense mutations. The positions of disorder-related polymorphisms or
667 mutations are highlighted in black spheres on the structures of ABCG5 (PDB ID: 5D07, chain C)
668 and ABCG8 (PDB ID 5D07, chain D). Structural motifs are indicated in dashed ovals: triple-
669 helical bundle (black), TMD polar relay (yellow), and extracellular domain with re-entry helices
670 (green). **B,** Microenvironment of G5-E146, G5-540, and G8-R543. *(Middle)* The transmembrane

671 domains (white) and the triple helical bundle (grey) are plotted in tube-styled cartoon
672 presentation, showing the α-carbons (spheres) of G5-E146 (orange), G8-R543 (blue), and G5-
673 A540 (black). The polar relays are plotted in dotted yellow spheres. *(Top-left)* Slapped top view
674 shows G5-A540 situated more than 10Å away from the polar relay of either subunit (red dot-
675 ended lines). *(Top-right)* Near G5-A540 shows a cholesterol-shaped electron density (mesh) in
676 the crystal structure of ABCG5/G8. Fo-Fc difference electron density map was contoured at
677 3.0σ. *(Bottom-left)* At the triple helical bundle of ABCG5, E146 interacts with R377 through
678 their side-chain termini in a distance of hydrogen bonding, 3.5Å (black dashed line). *(Bottom-*
679 *right)* In ABCG8 polar relay, R543 interacts E503 through their side-chain termini in a distance
680 of hydrogen bonding, 3.1Å (black dashed line).

681

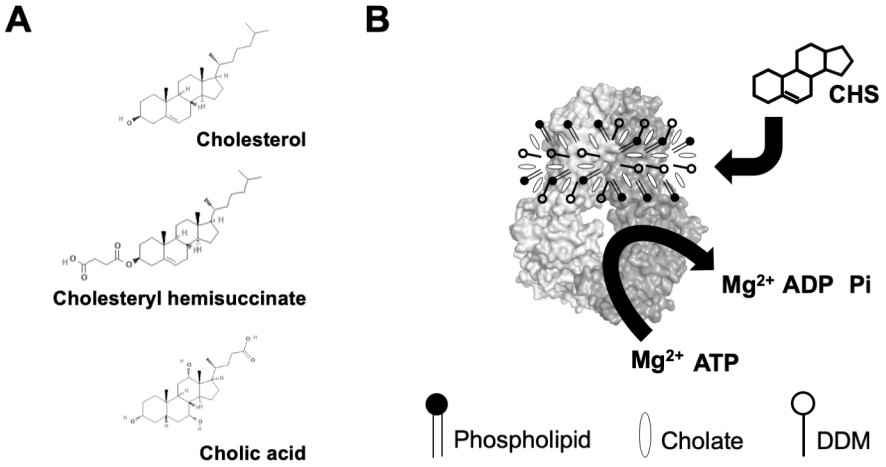

682

683 **Figure 2. A,** Chemical structures of cholesterol, cholesteryl hemisuccinate (CHS) and cholic
684 acid (cholate). Source: PubChem. **B,** Schematic illustration of sterol-coupled ATPase activity of
685 ABCG5/G8. DDM-purified ABCG5/G8 (light/dark grey surface) is preincubated with
686 phospholipids and cholate. Addition of CHS (four-ringed steroid structure) stimulates hydrolysis
687 of ATP to ADP and inorganic phosphate (Pi) in the presence of the divalent magnesium ions
688 (Mg^{2+}). Using the colorimetric and bismuth citrate-based assay, the liberated Pi is then captured
689 by ammonium molybdate in the presence ascorbic acid. The color is developed upon mixing
690 with bismuth citrate and sodium citrate, and the absorbance was measured at 695 nm. See details
691 in Materials and Methods.

692

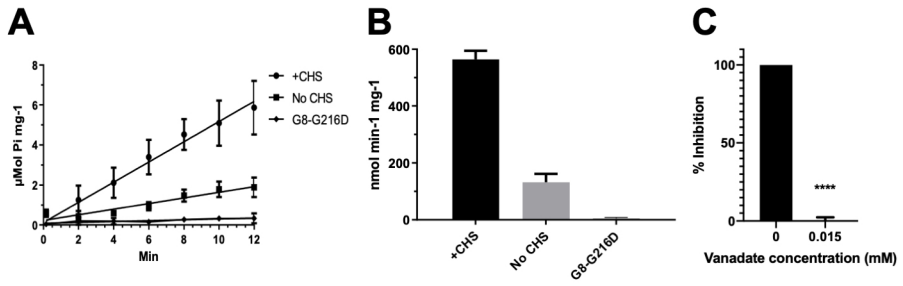

693

694 **Figure 3. ATPase activity of ABCG5/G8.** The ATP hydrolysis was used as a measure of
695 ABCG5/G8 ATPase activity at 37°C in a condition with 5mM ATP and 4.1mM CHS. The
696 protocol is entailed in Materials and Methods. **A,** Data points are presented as the means ±
697 standard deviations from 4-8 independent time-course experiments, where not visible, the error
698 bars are covered by the plot symbols. A linear regression, plotted from the first 12 minutes, is
699 used to calculate the specific activities. **B,** Bar graphs show the specific activities of ATP
700 hydrolysis by WT in the presence and absence of CHS and the catalytically deficient mutant G8-
701 G216D in the presence of CHS. The specific activity of WT in the absence of CHS is regarded as
702 the basal ABCG5/G8 ATPase activity. **C,** Bar graphs represent percentage inhibition of
703 ABCG5/G8 ATPase activity by 0.015mM orthovanadate, a P-value of <0.0001 obtained using
704 ordinary one-way ANOVA (Prism 8).

705

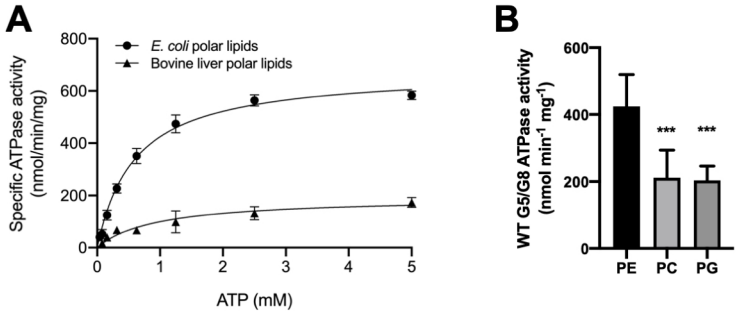

706

707 **Figure 4. Lipid dependence of ABCG5/G8 ATPase activity. A,** Purified ABCG5/G8 was
708 assayed in the presence of either *E. coli* or bovine liver polar lipids, and the specific activities of
709 ATP hydrolysis were obtained by the ATP concentration-dependent experiments (0-5mM ATP).
710 Both curves are fitted to the Michaelis-Menten equation (Prism 8), and the means of at least
711 three replicates along with standard deviations are plotted here. The kinetic parameters are listed
712 in Table 1. **B,** In a condition of 5mM ATP and 4.1mM CHS, ATP hydrolysis of purified
713 ABCG5/G8 was assayed in the presence of egg PE, soy PC or egg PG, a P-value of 0.0006 and
714 0.0003, respectively, obtained using ordinary one-way ANOVA (Prism 8).

715

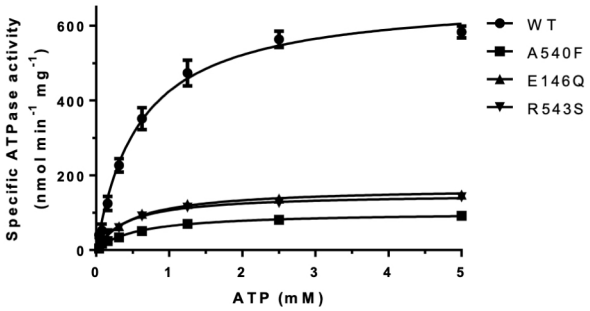

716

717 **Figure 5. ATP-Dependence of ABCG5/G8 ATPase Activity.** Purified proteins were assayed in
718 the presence of *E. coli* polar lipids, and the specific activities of ATP hydrolysis were obtained
719 by the ATP concentration-dependent experiments (0-5mM ATP). The curves are fitted to the
720 Michaelis-Menten equation (Prism 8), and the means of at least three replicates along with
721 standard deviations are plotted here. The kinetic parameters are listed in Table 1.

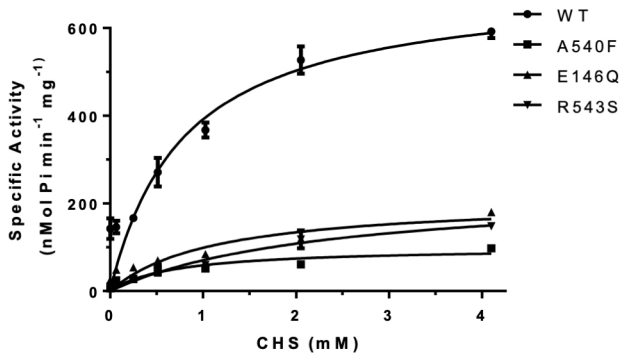

722

723 **Figure 6. CHS-Dependence of ABCG5/G8 ATPase Activity.** Purified proteins were assayed in
724 the presence of *E. coli* polar lipids, and the specific activities of ATP hydrolysis were obtained
725 by the CHS concentration-dependent experiments (0-4.1mM CHS). The curves are fitted to the
726 Michaelis-Menten equation (Prism 8), and the means of at least three replicates along with
727 standard deviations are plotted here. The kinetic parameters are listed in Table 2.

728

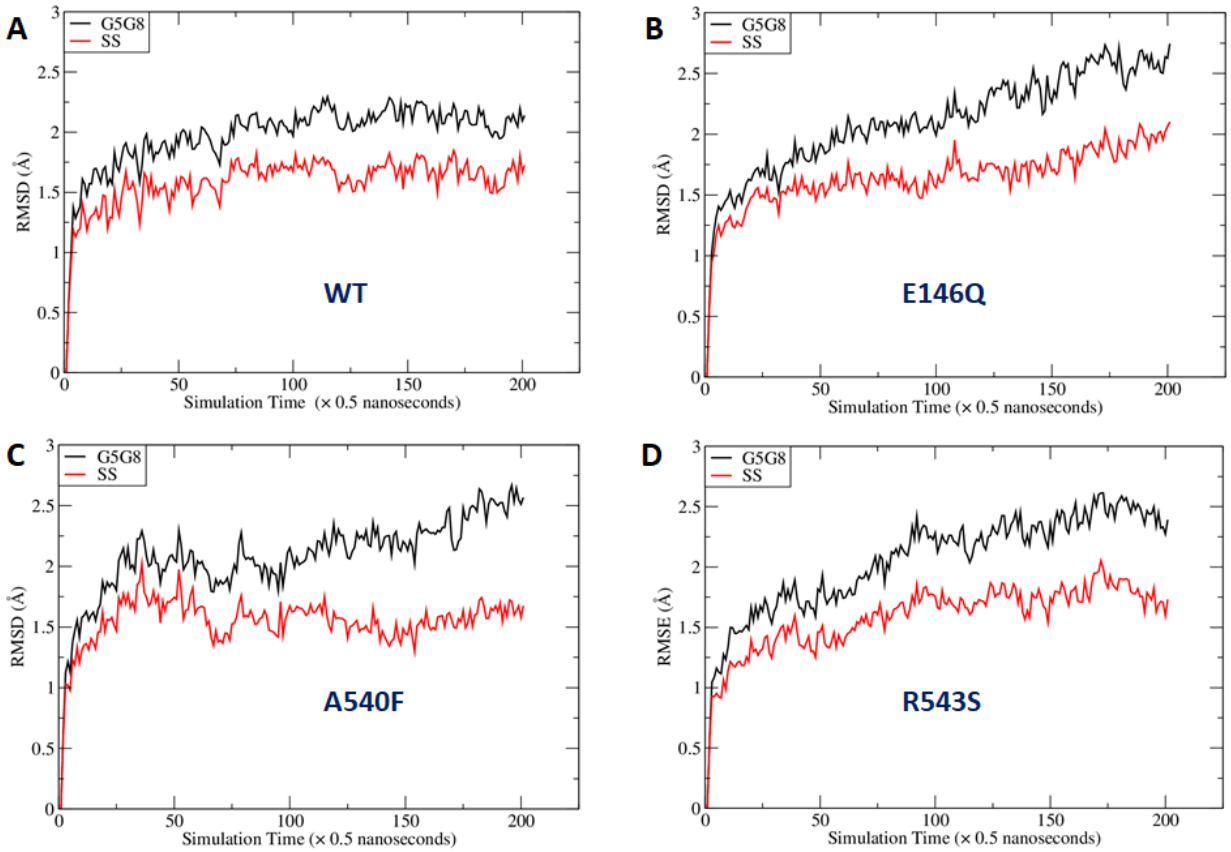

Figure 7. Fluctuation of Root-mean-square deviations (RMSD) along MD simulation time course. RMSD were calculated using the main chain atoms of all residues (black lines) or secondary structures only (red lines). A: wild type, B: E146Q mutant in ABCG5, C: A540F mutant in ABCG5, and D: R543S mutant in ABCG8. G5G8: ABCG5/G8; SS: secondary structure.

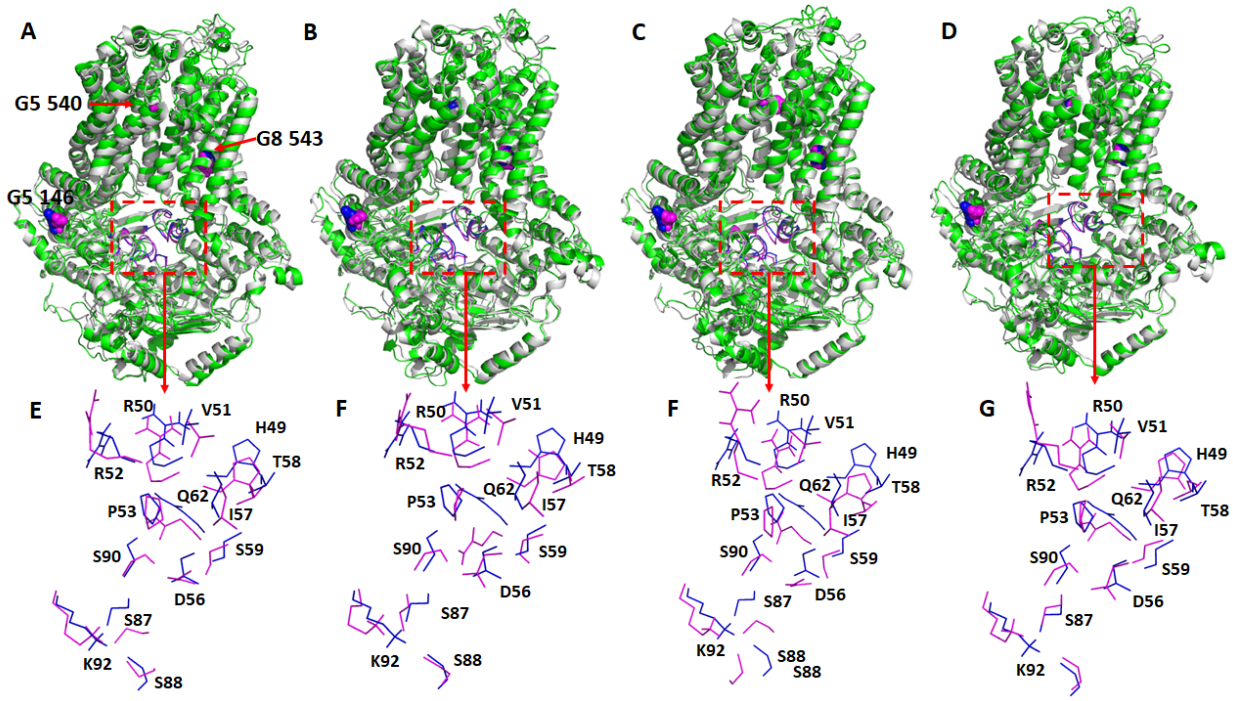

737

738 **Figure 8. Representative structures of the WT ABCG5/G8 and its three missense mutants.**

739 The representative structures (shown as green cartoons, magenta spheres and magenta lines)

740 were aligned to the crystal structure (grey cartoons, blue spheres and blue lines). The three

741 mutation residues, E146Q, A540F and R543S, are shown as spheres. The hypothetical

742 surrounding residues of ATP are shown as lines. A and E: wild type, B and F: E146A, C and F:

743 A540F, D and G: R543S. G5: ABCG5; G8: ABCG8.

744

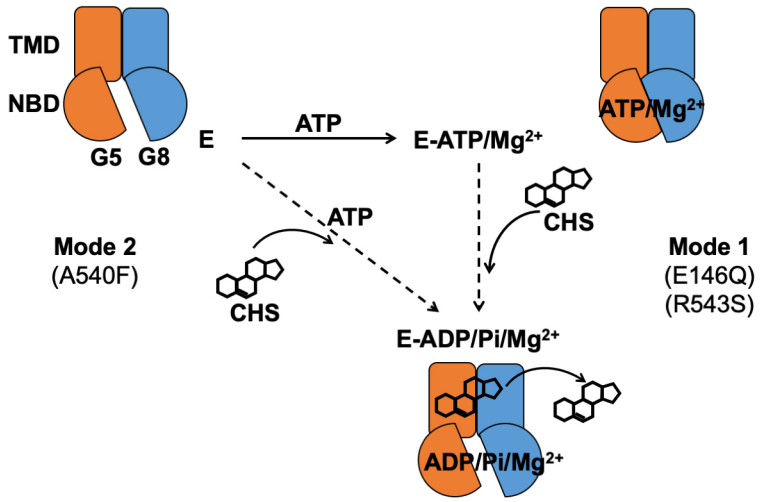

745

746 **Figure 9. Proposed mechanism of sterol-coupled ATP catalysis by ABCG5/G8.** *(Mode 1)* A
747 sequential pathway is derived from experiments on the disease mutants, G5-E146Q and G8-
748 R543S. ABCG5/G8 first recruits ATP and Mg^{2+} ions, likely causing a conformational change of
749 the NBD for ATP binding. CHS/sterol then binds the transporter and triggers ATP hydrolysis
750 that may result in its dissociation. *(Mode 2)* A concerted pathway is derived from experiments on
751 the putative sterol-binding mutant, G5-A540F. ABCG5/G8 simultaneously recruits CHS, ATP,
752 and Mg^{2+} ions, induces a transient conformational change of the NBD, and activates ATP
753 hydrolysis and CHS/sterol dissociation from the transporter. G5: ABCG5; G8: ABCG8; E:
754 ABCG5/G8 heterodimer; Pi: inorganic phosphate.

755

756 **Table 1.** Dependence of ABCG5/G8 ATPase Activity on ATP.

	V_{max}[a] (nmol/min/mg)	K_M (ATP) (mM)	k_{cat}[b] (s^{-1})	k_{cat}/K_M ($M^{-1}s^{-1}$)	$\Delta\Delta G_{MUT}$[c] (kJ/mol)
WT (liver polar lipids)	192.8 ± 17.9	0.93	0.48	0.52×10^3	-
WT (*E. coli* polar lipids)	677.1 ± 25.6	0.60	1.69	2.8×10^3	-
G5-E146Q[d]	167.1 ± 0.05	0.51	0.41	0.82×10^3	11.7
G8-R543S[d]	150.7 ± 3.7	0.42	0.38	0.90×10^3	12.3
G5-A540F[d]	101.2 ± 4.2	0.58	0.25	0.43×10^3	15.8

757 **a,** Standard errors were calculated from the fits shown in Figures 3A & 5D using GraphPad

758 Prism 8.

759 **b,** Turnover rates, k_{cat}, were calculated using the following formula. $V_{max} = k_{cat} \times [E]$, [E]: protein

760 concentration of ABCG5/G8 (363.1 nM).

761 **c,** Differential Gibbs free energy was calculated according to the formula: $\Delta\Delta G_{MUT} = -$

762 $RTln(k_{MUT}/k_{WT})$, k_{MUT}: k_{cat} of mutants, k_{WT}: k_{cat} of WT, R = 8.314 $Jmol^{-1}K^{-1}$ (R: Gas Constant, K:

763 Kelvin), T = 310.15 K (37°C).

764 **d,** Mutants were all assayed in the presence of *E. coli* polar lipids.

765

766 **Table 2.** Dependence of ABCG5/G8 ATPase Activity on Cholesteryl Hemisuccinate.

	V_{max}[a] (nmol/min/mg)	K_M (CHS) (mM)	k_{cat}[b] (s^{-1})	k_{cat}/K_M ($M^{-1}s^{-1}$)	$\Delta\Delta G_{MUT}$[c] (kJ/mol)
WT[d]	702.9 ± 50.7	0.8	1.74	2.2×10^3	-
G5-E146Q[d]	210.0 ± 33.2	1.13	0.52	0.46×10^3	10.0
G8-R543S[d]	237.1 ± 33.4	2.38	0.59	0.25×10^3	9.0
G5-A540F[d]	99.8 ± 11.4	0.70	0.25	0.36×10^3	16.1

767 **a,** Standard errors were calculated from the fits shown in Figures 3A & 5D using GraphPad

768 Prism 8.

769 **b,** Turnover rates, k_{cat}, were calculated using the following formula. $V_{max} = k_{cat} \times [E]$, [E]: protein

770 concentration of ABCG5/G8 (363.1 nM).

771 **c,** Differential Gibbs free energy was calculated according to the formula: $\Delta\Delta G_{MUT} = -$

772 $RTln(k_{MUT}/k_{WT})$, k_{MUT}: k_{cat} of mutants, k_{WT}: k_{cat} of WT, R = 8.314 $Jmol^{-1}K^{-1}$ (R: Gas Constant, K:

773 Kelvin), T = 310.15 K (37°C).

774 **d,** Both WT and mutants were assayed in the presence of *E. coli* polar lipids.

775

776 **SUPPLEMENTARY FIGURES**

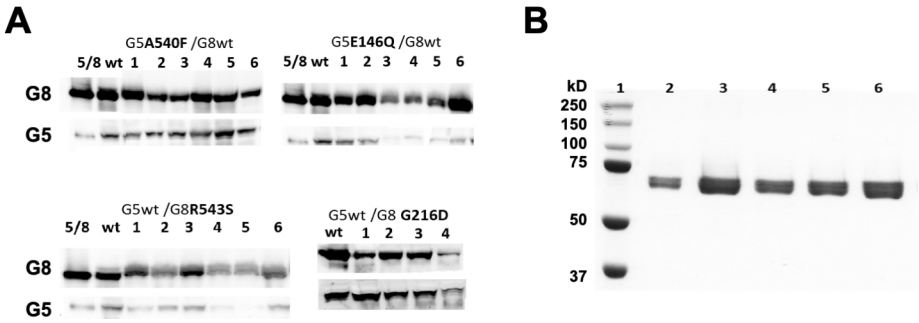

777

778 **Supplementary Figure 1. Expression and purification of ABCG5/G8 missense mutants. A,**
779 Four or six yeast colonies were selected for expression test. Crude microsomal membranes
780 (either WT or mutants), containing 20-30μg total proteins, were resolved by SDS–PAGE.
781 Protein expression was analyzed by Western blotting using a monoclonal anti-$RGSH_4$ antibody
782 to detect ABCG5 and a polyclonal anti-human ABCG8 antibody to detect ABCG8. The clones
783 expressing the highest level for both subunits were selected for protein purification. **B,** Gel-
784 filtration purified mutants were resolved on a 10% SDS-PAGE gel and stained by Coomassie
785 Blue (shown here in greyscale). Lanes 1: molecular weight marker, 2: G8-G216D, 3: G5-E146Q,
786 4: G8-R543S, 5: G5-A540F, and 6: WT.

787

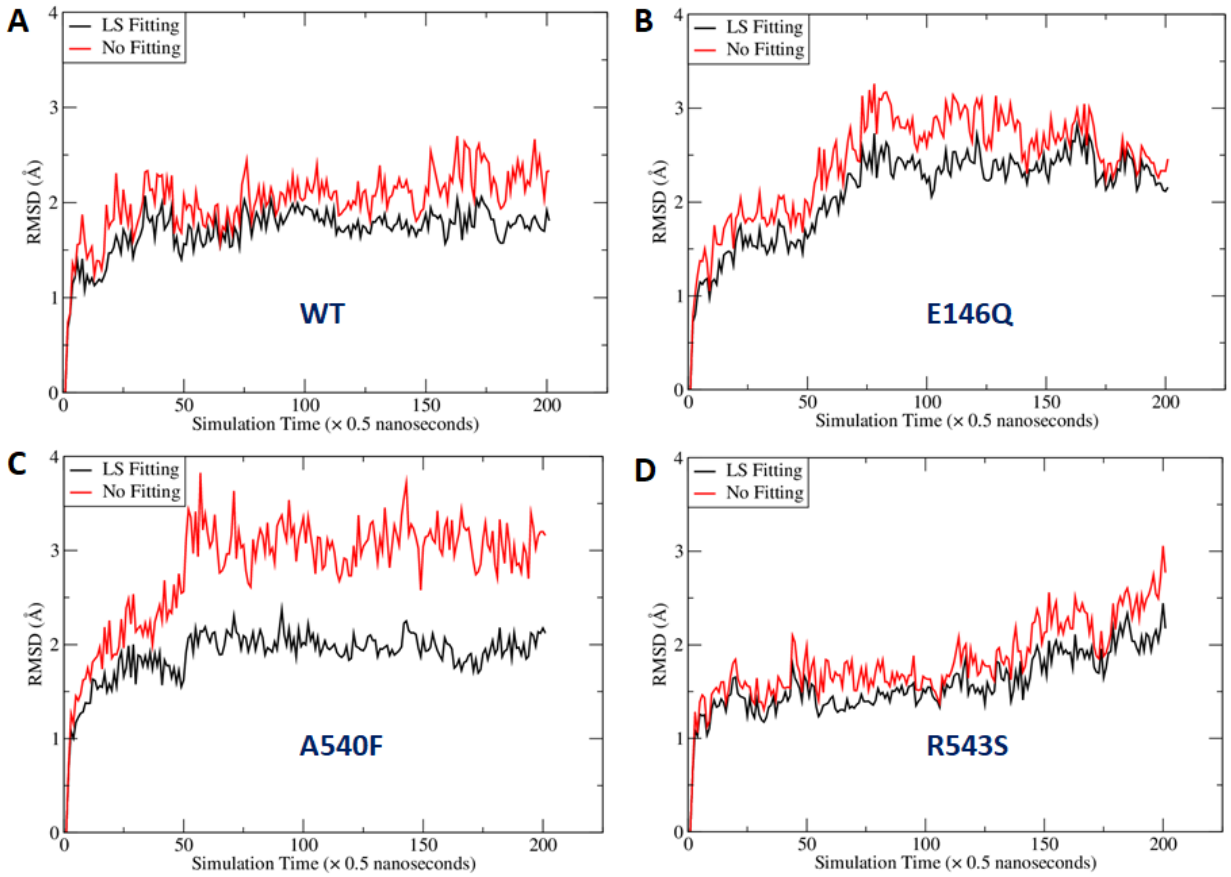

Supplementary Figure 2. Fluctuation of Root-mean-square deviations (RMSD) along MD simulation time course. RMSD were calculated for the hypothetical residues surrounding ATP under two scenarios. In the first scenario, least-square (LS) fittings were performed for the main chain atoms of the hypothetic residues which including Residues 48-62, 68, 86-94, 134, 218, 250, 251, 267, 268, 302 of G5 and 242-244 of G8. In the second scenario, the RMSD were calculated directly for the hypothetical residues without LS Fitting after the MD snapshots were aligned to the crystal structure using the secondary structures of ABCG5/G8. The fluctuations of the first and second scenarios were illustrated using black and red curves.